Ab initio k · p theory of spin-momentum locking: Application to topological surface states

I. A. Nechaev[1] and E. E. Krasovskii[2,3,4]

[1]*Department of Electricity and Electronics, FCT-ZTF, UPV-EHU, 48080 Bilbao, Spain*
[2]*Donostia International Physics Center, Paseo Manuel de Lardizabal 4, 20018 Donostia/San Sebastián, Basque Country, Spain*
[3]*Departamento de Polímeros y Materiales Avanzados: Física, Química y Tecnología, Universidad del Pais Vasco/Euskal Herriko Unibertsitatea, 20080 Donostia/San Sebastián, Basque Country, Spain*
[4]*IKERBASQUE, Basque Foundation for Science, 48013 Bilbao, Basque Country, Spain*

Based on *ab initio* relativistic k · p theory, we derive an effective two-band model for surface states of three-dimensional topological insulators up to seventh order in k. It provides a comprehensive description of the surface spin structure characterized by a nonorthogonality between momentum and spin. We show that the oscillation of the nonorthogonality with the polar angle of k with a $\pi/3$ periodicity can be seen as due to effective sixfold symmetric spin-orbit magnetic fields with a quintuple and septuple winding of the field vectors per single rotation of k. Owing to the dominant effect of the classical Rashba field, there remains a single-winding helical spin structure but with a periodic few-degree deviation from the orthogonal locking between momentum and spin.

I. INTRODUCTION

Over the last decade, the effective model Hamiltonian for topological surface states developed in Refs. [1,2] has been commonly accepted as a tool for including in a simple manner the remarkable features of these states: linear energy-momentum dispersion and helical in-plane spin structure. This model has been applied to a variety of topologically nontrivial materials in the spirit of the classical Rashba model, which, since the seminal paper by LaShell *et al.* [3], has been used to fit the two-dimensional (2D) spin-orbit split states at trivial surfaces. The spin-orbit splitting $k_\pm$-linear term is the same for trivial and for topological surface states, and it yields an orthogonal spin-momentum locking commonly considered a hallmark of a strong spin-orbit interaction (SOI).

The simplified model of Refs. [1,2] needs to be extended in order to describe the nonorthogonality between spin and momentum in realistic systems, as, e.g., observed in photoemission from Bi_2Se_3 [4]. While it naturally arises in *ab initio* calculations, in k · p theory, in order to yield a deviation from orthogonality, an effective Hamiltonian must include higher-order in k spin-orbit terms. In Ref. [5], for structures with the C_{3v} crystal symmetry and time-reversal symmetry it was suggested to include a $k_\pm^5$ term to allow for the nonorthogonality, and a minimal fifth-order k · p model was applied to Bi_2Te_3. Following Ref. [5], in Ref. [6] this model was also used to analyze the spin structure of the Au/Ge(111) surface state, which is rather far from being Rashba-like. Since the fifth-order Hamiltonian was constructed based on symmetry arguments rather than derived directly from *ab initio* spinor wave functions, its parameters were found by fitting to the *ab initio* band structure, which is an approximate procedure sensitive to the choice of the energy interval of interest and to the order of the k · p expansion: with each successive order the

complexity and ambiguity grow, and the parameters become increasingly less physically meaningful.

Here, we study the angle between the spin and momentum in the surface states of Bi_2Se_3 and Bi_2Te_2Se within our *ab initio* relativistic k · p approach introduced in Refs. [7–9]. This approach has been successfully applied to different materials [9–12] and established as a reliable theoretical tool for deriving few-band k · p Hamiltonians capable of comprehensive description of the surface spin structure. We take Bi_2Se_3 and Bi_2Te_2Se as vivid examples of the topological insulators (TIs) with a rather wide absolute bulk band gap bridged by the partly occupied topological surface state and a local projected gap well above the Fermi level hosting the so-called second topological surface state [13–17]. The wide gap is favorable for minimizing the effect of the proximity of bulk states on the surface-state spin structure. The presence of the second surface state makes it possible to derive a *two-band seventh-order* Hamiltonian by applying the Löwdin partitioning to a *four-band third-order* Hamiltonian generated for the two surface states within our *ab initio* approach.

For Bi_2Se_3 and Bi_2Te_2Se, we derive the seventh-order Hamiltonian allowing for the nonorthogonal locking between momentum and spin. We show that there is an oscillation of the spin around the momentum-perpendicular direction with a $\pi/3$ periodicity as a function of the polar angle of k due to the presence of k-dependent effective spin-orbit magnetic fields of the sixfold symmetry. The effective Hamiltonian facilitates the inclusion of the nonorthogonality in the description of spin-related properties of the TI surfaces and their interpretation within k · p theory. Thus, our paper can also be considered as an *ab initio* substantiation of the fifth-order Hamiltonian proposed in Ref. [4], based on an unambiguous algorithm for its parameters.
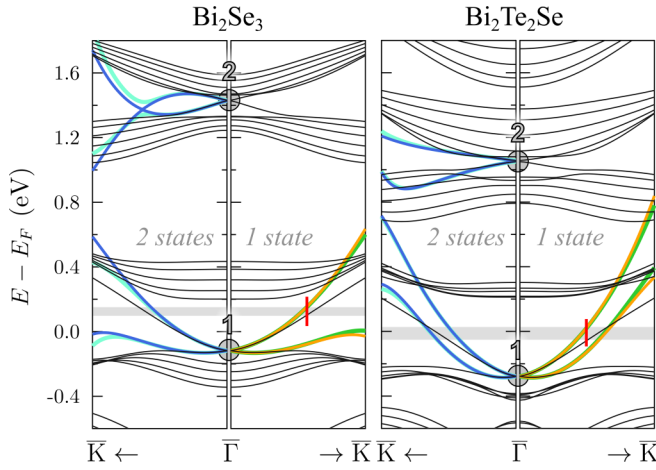
FIG. 1. Band structure of the surface of Bi_2Se_3 and Bi_2Te_2Se along $\bar{\Gamma}$-$\bar{K}$ by the full LDA Hamiltonian $H_{\mathbf{k}}^{LDA}$ (black lines), the 8×8 Hamiltonian (1) (light blue lines), the 4×4 Hamiltonian (2) (blue lines), and the 2×2 Hamiltonian (7) with two different values of $\tilde{\gamma}^{(7)}$ (green and orange lines, see text). The upper (lower) border of the horizontal stripes corresponds to the energy at which the model (*ab initio*) CECs shown in Fig. 2 are calculated. The **k** points on these CECs along $\bar{\Gamma}$-$\bar{K}$ are marked by vertical red lines.

II. COMPUTATIONAL DETAILS

The *ab initio* band structure is obtained with the extended linear augmented plane-wave method [18] (the accuracy of the wave functions is essential for the efficiency of our **k** · **p** methods) using the full potential scheme of Ref. [19] within the local density approximation (LDA). The spin-orbit interaction was treated as a second variation [20]. The surfaces

of the TIs are simulated by bulk-truncated centrosymmetric six-quintuple-layer (QL) slabs of space group $P\bar{3}m1$ (no. 164). The experimental crystal lattice parameters were taken from Ref. [21]. In the case of Bi_2Te_2Se, the experimental atomic positions of Ref. [21] were used, while for Bi_2Se_3 we took the LDA relaxed atomic positions of Ref. [22].

III. SPIN-MOMENTUM LOCKING ANGLE

Figure 1 shows the calculated LDA band structure of the Bi_2Se_3 and Bi_2Te_2Se surfaces along $\bar{\Gamma}$-$\bar{K}$. Two topological surface states are clearly identified in the spectra of both TIs. The two states are numbered $n = 1$ and 2 in order of increasing energy. The spin-resolved constant energy contours (CECs) at ≈ 0.2 eV above the Dirac points of the low-energy surface states ($n = 1$) are shown in Fig. 2 together with the respective angles of deviation from the orthogonal spin-momentum coupling δ. As a function of the polar angle $\varphi_{\mathbf{k}}$ of the momentum **k**, the deviation angle demonstrates an oscillating behavior with a $\pi/3$ periodicity and an amplitude close to $1.5°$ for Bi_2Se_3, which is in good agreement with the experiment of Ref. [4], and about $3.0°$ for Bi_2Te_2Se.

We start with a **k** · **p** Hamiltonian in the basis of the two Dirac surface states $n = 1$ and 2. Being eigenfunctions of a centrosymmetric slab Hamiltonian at $\bar{\Gamma}$, these states form four Kramers-degenerate pairs with spinor wave functions $\Psi_{m\mu}$, which we group into two twin pairs with two members, $m = 2n - 1$ and $2n$. Here, $\mu = \uparrow$ or $\downarrow$ indicates the sign $+$ or $-$ of the expectation value $\langle \Psi_{m\mu} | \hat{J}_z | \Psi_{m'\mu'} \rangle_\tau = \langle J_z \rangle_{m\mu} \delta_{mm'} \delta_{\mu\mu'}$ of the z projection of the total angular momentum $\hat{\mathbf{J}}$ at the (symmetry equivalent) atomic sites of type τ, which has the largest weight $\langle \Psi_{m\mu} | \Psi_{m\mu} \rangle_\tau$ (see Ref. [7]). The integration is
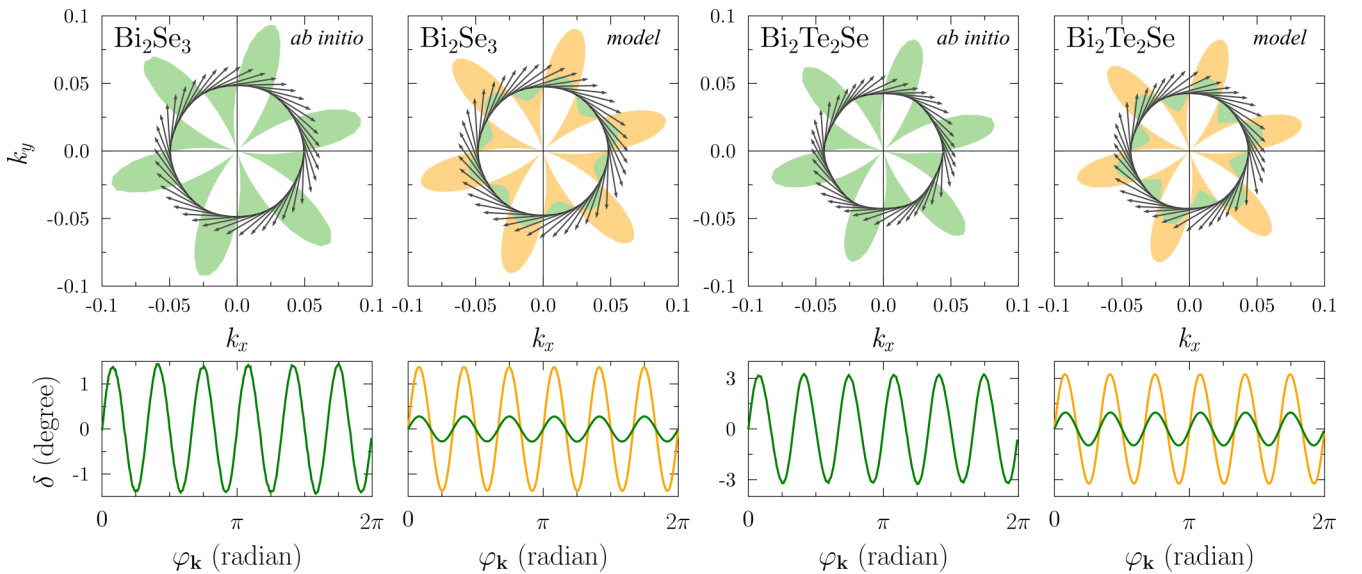
FIG. 2. Spin-resolved constant energy contours (upper panels) and the nonorthogonality δ as a function of the polar angle $\varphi_{\mathbf{k}}$ (lower panels) for Bi_2Se_3 and Bi_2Te_2Se. In the upper panels, the colored areas highlight the deviation of the in-plane spin direction from the classical Rashba in-plane spin at a given **k** point in the contour: the border of the areas is given by the length of the relevant **k** plus a scaled **k** projection of the in-plane spin: $k + R \sin \delta$, R being the scaling factor. The green areas and lines correspond to the LDA and **k** · **p** calculations, while the orange ones correspond to the **k** · **p** calculations with the magnitude of $\gamma^{(5)}$ manually increased by a factor of 4.5 for Bi_2Se_3 and of 3.8 for Bi_2Te_2Se (see text). The contours are calculated at the energies marked in Fig. 1.

over the muffin-tin spheres of this type, and the positive value is $\langle J_z \rangle_{m\uparrow} = -\langle J_z \rangle_{m\downarrow}$. With this basis set, we first microscopically derive an eight-band **k · p** Hamiltonian H_{kp} from an *ab initio* relativistic **k · p** perturbation expansion around the Γ point. The expansion is carried out up to the third order in **k** by applying the Löwdin partitioning [23–25] to the original Hilbert space of the Γ-projected LDA Hamiltonian $H_\mathbf{k}^{\text{LDA}}$ (see Appendix A).

Because $\Psi_{m\mu}$ are slab eigenfunctions representing the surface states, each twin pair is characterized by two doubly degenerate slab levels E_{2n-1} and E_{2n} separated by $\Delta_n = E_{2n} - E_{2n-1}$ of a few meV to the bonding-antibonding interaction. Since the $\bar\Gamma$ point is a time-reversal invariant momentum (TRIM), the spinors $\Psi_{m\mu}$ are also parity eigenfunctions, and the two pairs for a given $n = 1$ or 2 have different parity. We now transfer to a new basis $|\Phi_{n\mu}^{\pm}\rangle = \frac{1}{\sqrt{2}}[|\Psi_{2n-1\mu}\rangle \pm |\Psi_{2n\mu}\rangle]$, where the new basis functions $|\Phi_{n\mu}^{\pm}\rangle$ are no longer eigenfunctions but are localized at one of the two surfaces of the 6QL slab, "+" or "−." In this surface-resolved basis, the original 8×8 Hamiltonian reads

$$H_{\mathbf{kp}} \longrightarrow H_{\mathbf{kp}}^{\text{Film}} = \begin{pmatrix} H_{\text{Surf}}^{+} & H_{\text{int}} \\ H_{\text{int}}^{\dagger} & H_{\text{Surf}}^{-} \end{pmatrix}. \tag{1}$$

In Fig. 1, the bands obtained by diagonalizing this Hamiltonian are shown by light blue lines for both TIs.

Further we neglect the coupling of the surfaces due to the overlap between the + and − new basis functions, $H_{\text{int}} \to 0$, and in the following we will consider only the − surface, so we omit the superscript −. In a compact form, the resulting 4×4 Hamiltonian, which is just the term H_{Surf}^{-} of the Hamiltonian (1), reads

$$H_{\mathbf{kp}}^{4\times4} = \begin{pmatrix} E_1 + H_1 + H_1^{\text{R}} & H_0 + \widetilde{H} \\ H_0 + \widetilde{H}^{\dagger} & E_2 + H_2 + H_2^{\text{R}} \end{pmatrix}. \tag{2}$$

Here, each term of the diagonal and nondiagonal blocks is a 2×2 matrix, the implicit form of which directly follows from the *ab initio* **k · p** expansion up to the third order in **k**: $E_n = \epsilon_n \mathbb{I}_{2\times2}$, with $\mathbb{I}_{2\times2}$ being the 2×2 identity matrix, $H_n = M_n k^2 \mathbb{I}_{2\times2}$, $k = \sqrt{k_x^2 + k_y^2}$, and

$$H_n^{\text{R}} = \begin{pmatrix} -iW_n(k_+^3 - k_-^3) & i\tilde\alpha_n k_- \\ -i\tilde\alpha_n k_+ & iW_n(k_+^3 - k_-^3) \end{pmatrix}, \tag{3}$$

where $\tilde\alpha_n = \alpha_n^{(1)} + \alpha_n^{(3)} k^2$ and $k_\pm = k_x \pm k_y$ with k_x directed along $\bar\Gamma$-$\bar M$. The well-known 2×2 Rashba term H_n^{R} is responsible for the out-of-plane and in-plane spin structure typical of hexagonal structures (see, e.g, Ref. [9] and references therein). The interaction between the states $n = 1$ and 2 is realized through the term

$$\widetilde{H} = \begin{pmatrix} i\theta k_+^3 + i\eta k_-^3 & i\tilde\zeta k_- + Dk_-^2 \\ -i\tilde\zeta k_+ - Dk_-^2 & i\theta k_-^3 + i\eta k_+^3 \end{pmatrix} \tag{4}$$

with $\tilde\zeta = \zeta^{(1)} + \zeta^{(3)} k^2$.

TABLE I. Parameters of the four-band Hamiltonians (2) (based on calculations for 6QL-layer slabs with the lattice parameter $a = 7.8187$ a.u. for Bi_2Se_3 and $a = 8.0880$ a.u. for Bi_2Te_2Se). All parameters are in Rydberg atomic units except for ϵ_1 and ϵ_2 presented in eV.

	Bi_2Se_3	Bi_2Te_2Se
ϵ_1	−0.118	−0.278
ϵ_2	1.429	1.053
$\alpha_1^{(1)}$	0.174	0.187
$\alpha_2^{(1)}$	−0.265	−0.150
$\alpha_1^{(3)}$	28.30	−29.03
$\alpha_2^{(3)}$	141.80	−22.35
θ	8.33	22.39
η	−1.02	−3.00
$\zeta^{(1)}$	−0.048	−0.078
$\zeta^{(3)}$	−52.83	4.51
D	−2.64	−3.40
M_1	7.97	15.67
M_2	−2.56	−1.76
M_0	−0.37	0.61
W_1	−4.71	−17.32
W_2	5.53	11.88
$s_1^{\parallel}$	0.70	0.63
$s_2^{\parallel}$	0.42	0.39
s_1^z	0.40	0.26
s_2^z	−0.16	−0.21
$\tilde s^{\parallel}$	−0.21	−0.10
$\tilde s^z$	−0.41	−0.20

In the new basis, the spin matrix that yields the spin structure of the states under study is defined as

$$\mathbf{S}_{\mathbf{kp}}^{4\times4} = \begin{pmatrix} \mathbf{S}_1 & \widetilde{\mathbf{S}} \\ \widetilde{\mathbf{S}} & \mathbf{S}_2 \end{pmatrix} \tag{5}$$

with $\mathbf{S}_n = (s_n^{\parallel}\boldsymbol{\sigma}_{\parallel}, s_n^z \sigma_z)$ and $\widetilde{\mathbf{S}} = (\tilde s^{\parallel}\boldsymbol{\sigma}_{\parallel}, \tilde s^z \sigma_z)$, where $\boldsymbol{\sigma}_{\parallel} = (\sigma_x, \sigma_y)$ and σ_x, σ_y, and σ_z are the Pauli matrices. The elements of the spin matrix $[\mathbf{S}_{\mathbf{kp}}^{4\times4}]_{l\nu}^{n\mu} = \langle \Phi_{n\mu}|\boldsymbol{\sigma}|\Phi_{l\nu}\rangle$ enter into the expression for the spin expectation value

$$\langle \mathbf{S}_{\mathbf{k}\lambda}\rangle = \frac{1}{2}\langle \widetilde\Phi_\mathbf{k}^\lambda | \boldsymbol{\sigma} | \widetilde\Phi_\mathbf{k}^\lambda\rangle = \frac{1}{2}\sum_{n\mu l\nu} C_{\mathbf{k}n\mu}^{\lambda*} C_{\mathbf{k}l\nu}^{\lambda} [\mathbf{S}_{\mathbf{kp}}^{4\times4}]_{l\nu}^{n\mu} \tag{6}$$

in the state $|\widetilde\Phi_\mathbf{k}^\lambda\rangle = \sum_{n\mu} C_{\mathbf{k}n\mu}^{\lambda}|\Phi_{n\mu}\rangle$ of the reduced Hilbert space of the Hamiltonian $H_{\mathbf{kp}}^{4\times4}$. The four-dimensional vectors $\mathbf{C}_\mathbf{k}^\lambda$ diagonalize this Hamiltonian $H_{\mathbf{kp}}^{4\times4}\mathbf{C}_\mathbf{k}^\lambda = E_\mathbf{k}^\lambda \mathbf{C}_\mathbf{k}^\lambda$. The parameters in Eqs. (2) and (5) are listed in Table I. The bands obtained with these parameters are shown in Fig. 1 by blue lines.

Next, we *analytically* transform the Hamiltonian (2) by means of the Löwdin partitioning, retaining terms up to seventh order in **k** for the block $E_1 + H_1 + H_1^{\text{R}}$ of this Hamiltonian. As a result, we arrive at the 2×2 Hamiltonian that describes the low-energy Dirac surface state:

$$H_{\mathbf{kp}}^{2\times2} = \begin{pmatrix} \epsilon_1 + \mathcal{M}k^2 - i\mathcal{W}(k_+^3 - k_-^3) + \mathcal{N}(k_+^6 + k_-^6) & i\tilde\alpha k_- - i\tilde\gamma k_+^5 + i\xi k_-^7 \\ -i\tilde\alpha k_+ + i\tilde\gamma k_-^5 - i\xi k_+^7 & \epsilon_1 + \mathcal{M}k^2 + i\mathcal{W}(k_+^3 - k_-^3) + \mathcal{N}(k_+^6 + k_-^6) \end{pmatrix}, \tag{7}$$

TABLE II. Parameters of the two-band Hamiltonians (7) in Rydberg atomic units. The parameters ϵ_1, $\alpha_1^{(1)}$, $s_1^{\parallel}$, and s_1^z and the lattice parameter a are listed in Table I.

	Bi_2Se_3	Bi_2Te_2Se
$\alpha^{(3)}$	27.91	−28.27
$\alpha^{(5)}$	−575.48	115.57
$\alpha^{(7)}$	−92731.72	63344.71
$\gamma^{(5)}$	529.40	1735.90
$\gamma^{(7)}$	−39773.06	319791.93
ξ	51.10	589.48
$\mathcal{N}$	−157.85	−789.83
$\mathcal{M}^{(0)}$	7.95	15.61
$\mathcal{M}^{(2)}$	−110.14	−122.40
$\mathcal{M}^{(4)}$	−36925.53	−27778.63
$\mathcal{W}^{(0)}$	−5.82	−20.03
$\mathcal{W}^{(2)}$	−1389.00	−162.47
$\mathcal{W}^{(4)}$	−111467.25	65344.75

where $\mathcal{M} = \sum_{m=0}^{2} M^{(2m)}k^{2m}$, $\mathcal{W} = \sum_{m=0}^{2} W^{(2m)}k^{2m}$, $\tilde{\alpha} = \alpha_1^{(1)} + \sum_{m=1}^{3} \alpha^{(2m+1)}k^{2m}$, and $\tilde{\gamma} = \gamma^{(5)} + \gamma^{(7)}k^2$ (see Appendix B). All the parameters are listed in Table II. With these parameters, the diagonalization of the Hamiltonian (7) yields the bands shown by green lines in Fig. 1.

Up to fifth order in $\mathbf{k}$, the Hamiltonian (7) of our *ab initio* $\mathbf{k} \cdot \mathbf{p}$ theory is in accord with the form of the two-band Hamiltonian constructed in Ref. [5] for Bi_2Te_3 considering the C_{3v} crystal symmetry and time-reversal symmetry. In Ref. [6], the Hamiltonian of Ref. [5] was modified by adding a sixth-order term $k_+^6 + k_-^6$ in order to reproduce the hexagonal warping of the Au/Ge(111) surface state not related to the spin-orbit effect. Obviously, this term is naturally present in our theory. Note that in Refs. [5,6] the values of the parameters were found by fitting the model Hamiltonian to *ab initio* results, and, for example, in the case of the surface state of Bi_2Te_3 [5] the values for the lower-order terms differ strongly from those obtained in Refs. [2,7], which are currently commonly accepted. In contrast to a fitting method, in our $\mathbf{k} \cdot \mathbf{p}$ theory the shape and the value of a given order term are independent

of whether or not we include higher-order terms (and it does not affect the lower-order terms), since our $\mathbf{k} \cdot \mathbf{p}$ expansion uniquely follows from the basis set—the eigenfunctions of the original *ab initio* Hamiltonian.

The spin-resolved CECs and the nonorthogonality by our $\mathbf{k} \cdot \mathbf{p}$ model are shown in Fig. 2. As seen in the figure, the effective model underestimates the nonorthogonality for the lower-energy Dirac surface states. A better agreement with the respective *ab initio* results is achieved by increasing the magnitude of $\gamma^{(5)}$ by a factor of 4.5 ($\gamma^{(5)} = 2382.3$ a.u.) and 3.8 ($\gamma^{(5)} = 6596.4$ a.u.) for Bi_2Se_3 and Bi_2Te_2Se, respectively (see the orange areas and curves in Fig. 2; the respective energy bands are shown by orange lines in Fig. 1). Note that by manually correcting this parameter we reproduce more accurately not only the nonorthogonality, but also the hexagonal warping of the contours.

IV. EFFECTIVE FIELDS AND MULTIPLE WINDING

We focus now on the terms of the 2×2 Hamiltonian that cause the nonorthogonality in the in-plane-spin structure. We rewrite the Hamiltonian (7) in terms of the Pauli matrices:

$$H_{\mathbf{kp}}^{2\times2} = \mathcal{E}(\mathbf{k})\sigma_0 + \boldsymbol{\mathcal{B}} \cdot \boldsymbol{\sigma}, \tag{8}$$

where $\mathcal{E}(\mathbf{k}) = \epsilon_1 + \mathcal{M}k^2 + 2\mathcal{N}k^6 \cos 6\varphi_{\mathbf{k}}$ represents the dispersion of the doubly degenerate bands with the hexagonal warping of their CECs. The SOI-induced splitting of the bands

$$E^{\pm}(\mathbf{k}) = \mathcal{E}(\mathbf{k}) \pm |\boldsymbol{\mathcal{B}}| \tag{9}$$

is due to the Zeeman-like term with the effective (spin-orbit) magnetic field:

$$\boldsymbol{\mathcal{B}} = \tilde{\alpha}\boldsymbol{\mathcal{B}}_{R}^{(1)} + 2\mathcal{W}\boldsymbol{\mathcal{B}}_{Z}^{(3)} + \tilde{\gamma}\boldsymbol{\mathcal{B}}^{(5)} + \xi\boldsymbol{\mathcal{B}}^{(7)}. \tag{10}$$

This field consists of the classical (linear) Rashba magnetic field $\boldsymbol{\mathcal{B}}_{R}^{(1)} = k(\sin\varphi_{\mathbf{k}}, -\cos\varphi_{\mathbf{k}}, 0)$, the cubic field $\boldsymbol{\mathcal{B}}_{Z}^{(3)} = k^3(0, 0, \sin 3\varphi_{\mathbf{k}})$ responsible for the well-known threefold symmetric pattern of the spin z component and contributing to the hexagonal warping of the CECs [26], and two higher-order sixfold symmetric fields $\boldsymbol{\mathcal{B}}^{(5)} = k^5(\sin 5\varphi_{\mathbf{k}}, \cos 5\varphi_{\mathbf{k}}, 0)$ and $\boldsymbol{\mathcal{B}}^{(7)} = k^7(\sin 7\varphi_{\mathbf{k}}, -\cos 7\varphi_{\mathbf{k}}, 0)$ (see Fig. 3). Note that since the spin matrix $(s_1^{\parallel}\boldsymbol{\sigma}_{\parallel}, s_1^z\sigma_z)$ of our two-band $\mathbf{k} \cdot \mathbf{p}$ model [the upper-left 2×2 block of the spin matrix (5)] differs from the matrix $(\boldsymbol{\sigma}_{\parallel}, \sigma_z)$ of a model built on a scalar-relativistic basis only by the nonunity coefficients $s_1^{\parallel}$ and s_1^z, one is tempted to treat the Pauli matrices in Eq. (8) as if they were spin matrices. Then, the spin expectation value is $\mathbf{S}^{\pm}(\mathbf{k}) = \pm\frac{1}{2}\boldsymbol{\mathcal{B}}/|\boldsymbol{\mathcal{B}}|$. However, irrespective of the interpretation of $\boldsymbol{\sigma}$ in Eq. (8), in our model the nonorthogonality is characterized by the deviation angle $\delta^{\pm}$ found from the dot product:

$$\sin\delta^{\pm} = \frac{\mathbf{S}_{\parallel}^{\pm}(\mathbf{k}) \cdot \mathbf{k}}{|\mathbf{S}_{\parallel}^{\pm}(\mathbf{k})|k} = \pm\frac{k^5}{|\boldsymbol{\mathcal{B}}_{\parallel}|}(\tilde{\gamma} + \xi k^2)\sin 6\varphi_{\mathbf{k}}, \tag{11}$$

where the parallel (in-plane) component of the effective field (10) is

$$\begin{aligned} |\boldsymbol{\mathcal{B}}_{\parallel}|^2 = {} & (\tilde{\alpha}^2 + \tilde{\gamma}^2 k^8 + \xi^2 k^{12})k^2 \\ & - 2\tilde{\alpha}k^6(\tilde{\gamma} - \xi k^2)\cos 6\varphi_{\mathbf{k}} \\ & - 2\tilde{\gamma}\xi k^{12}\cos 12\varphi_{\mathbf{k}}. \end{aligned} \tag{12}$$

FIG. 3. Effective spin-orbit magnetic fields in Eq. (10) as a function of polar angle $\varphi_{\mathbf{k}}$. The in-plane fields $\boldsymbol{\mathcal{B}}_{R}^{(1)}$, $\boldsymbol{\mathcal{B}}^{(5)}$, and $\boldsymbol{\mathcal{B}}^{(7)}$ are represented by arrows showing the direction of the field vectors at a given $\mathbf{k}$. The out-of-plane field $\boldsymbol{\mathcal{B}}_{Z}^{(3)}$ is illustrated by the blurred 60° sectors of green and orange color for the negative and positive sign of its z projection, respectively.

We see that the angle $\delta^{\pm}$ has a nontrivial dependence on the polar angle with a $\pi/3$ periodicity due to the presence of the fields $\mathcal{B}^{(5)}$ and $\mathcal{B}^{(7)}$. Acting separately, these fields may cause a quintuple or a septuple winding of the in-plane spin, respectively, in contrast to the Rashba field $\mathcal{B}_{R}^{(1)}$ yielding a single winding. In Fig. 3 each in-plane effective field is represented by arrows depicting the field vector at a set of **k** points on a circle. As seen in the figure, the vector of a field rotates anticlockwise [$\mathcal{B}^{(1)}_{R}$ and $\mathcal{B}^{(7)}$] or clockwise [$\mathcal{B}^{(5)}$] in moving anticlockwise along the circle. From one to the next red point, the field vector rotates by 2π, so we see one, five, and seven complete 2π rotations for $\mathcal{B}_{R}^{(1)}$, $\mathcal{B}^{(5)}$, and $\mathcal{B}^{(7)}$, respectively, referred to as a single, quintuple, and septuple winding.

At a given **k**, the importance of each contribution to the effective magnetic field of Eq. (10) depends on the respective parameter of the Hamiltonian (7): $\widetilde{\alpha}$, $\mathcal{W}$, $\widetilde{\gamma}$, or ξ. According to their values in Table II, the effect of the field $\mathcal{B}^{(7)}$ is expected to be negligible, because ξ is much smaller than $\alpha^{(7)}$ and $\gamma^{(7)}$. At the same time, the contribution of $\mathcal{B}^{(5)}$ depends on the parameters $\gamma^{(5)}$ and $\gamma^{(7)}$, which are comparable to or even larger than $\alpha^{(5)}$ and $\alpha^{(7)}$, respectively. However, because of the dominant contribution of the linear Rashba field $\mathcal{B}_{R}^{(1)}$ due to the rather large $\alpha_{1}^{(1)}$ in $\widetilde{\alpha}$ of Eq. (10), the superposition of all the in-plane fields produces a single winding of the in-plane spin [27].

The in-plane-field contribution (12) as well as the out-of-plane contribution $|\mathcal{B}_{Z}|^{2} = 2\mathcal{W}^{2}k^{6}(1 - \cos 6\varphi_{\mathbf{k}})$ of the effective field (10) affects the eigenvalues (9) of the Hamiltonian (8) though the splitting term $\pm|\mathcal{B}|$. This means that the SOI-induced hexagonal warping of the CECs is due not only to the cubic field $\mathcal{B}_{Z}$ as, e.g., in Ref. [26], but also to the fields $\mathcal{B}^{(5)}$ and $\mathcal{B}^{(7)}$, which contribute to the warping through the scalar products $\mathcal{B}^{(5)} \cdot \mathcal{B}_{R}^{(1)}$ and $\mathcal{B}^{(7)} \cdot \mathcal{B}_{R}^{(1)}$ [the terms proportional to $\widetilde{\alpha}\widetilde{\gamma}$ and $\widetilde{\alpha}\xi$ in Eq. (12), respectively]. As follows from Tables I and II, the fields $\mathcal{B}_{\shortparallel}$ and $\mathcal{B}_{Z}$ are equally important for the $\cos 6\varphi_{\mathbf{k}}$ distortion of the CEC. In addition, the hexagonal warping due to $\mathcal{B}_{Z}$ gives rise to the z spin component, so if one neglects the contribution of $\mathcal{B}_{\shortparallel}$ and fits only the cubic field to calculated or measured CECs one may arrive at a large out-of-plane spin polarization with the spin-momentum locking unaffected by the warping. In contrast, the CEC warping caused by the fields $\mathcal{B}^{(5)}$ and $\mathcal{B}^{(7)}$ is accompanied by a change of the locking angle between spin and momentum. This explains why a stronger warping may imply a larger nonorthogonality.

V. CONCLUSIONS

To summarize, within a fully *ab initio* **k** · **p** perturbation approach we have developed a two-band effective **k** · **p** model for the surface states of the three-dimensional topological insulators Bi_2Se_3 and Bi_2Te_2Se. The model includes terms to seventh order in **k** and provides a comprehensive description of the surface spin structure characterized by a nonorthogonality between the surface-electron spin and its momentum. In the **k** · **p** theory, the nonorthogonality that arises naturally in the *ab initio* calculations is included in the effective models through the higher-order terms in **k**. Our **k** · **p** expansion builds on the eigenfunctions of the *ab initio* Hamiltonian, and, therefore, a term of a given order is unambiguously

determined by the *ab initio* spinor wave functions and, in contrast to a fitting method, does not depend on the presence of other terms. We have shown that the $k_{\pm}^{5}$ and $k_{\pm}^{7}$ terms represent effective spin-orbit magnetic fields with six-fold symmetric patterns on the two-dimensional momentum plane and, thereby, can lead to a nonorthogonality with the $\pi/3$ periodicity as a function of the polar angle of **k**. For Bi_2Se_3 and Bi_2Te_2Se, we have found that the contribution of the $k_{\pm}^{7}$ term is rather small, and it is the $k_{\pm}^{5}$ term that causes the few-degree deviation of the actual spin direction from the classical orthogonality.

The present **k** · **p** theory extends the effective Hamiltonian approach to include the spin-momentum nonorthogonality via material-specific parameters of a 2×2 matrix. In contrast to the simpler versions that are limited to the description of the energy splitting and CEC warping, the higher-order parameters cannot be inferred from a fitting to a known result, but they can be *microscopically* derived from the *ab initio* band structure. Experimentally, the spin-momentum nonorthogonality may manifest itself in the anisotropy of the Edelstein effect and in opto-spintronic phenomena, and its knowledge is important to understand spin-resolved photoemission.

Finally, we would like to note that the derived two-band Hamiltonian is fully applicable to classical Rashba systems such as the Au(111) surface state. Here, the nonorthogonality appears to be negligibly small, albeit nonzero. A similar study for the giant Rashba spin-split conduction state of a single BiTeI trilayer reveals a substantial nonorthogonality, rather different for the inner and outer constant energy contour. In fact, the two-band Hamiltonian (7) can be considered typical of hexagonal structures. Thus, the simplified picture that the in-plane spin and momentum are locked perpendicular to each other by spin-orbit interaction might overlook important features inherent in the spin-related phenomena at the surfaces and in 2D structures.

APPENDIX A: *AB INITIO* THIRD-ORDER **k** · **p** EXPANSION

The Löwdin partitioning applied to the original Hilbert space of the LDA Hamiltonian represents the **k** · **p** Hamiltonian in the basis of the chosen spinor wave functions (the states in set A numbered below by the indices $n\nu$, $m\mu$, and $m'\mu'$) in terms of the matrix elements of the velocity operator [7,28]

$$\boldsymbol{\pi} = -i\hbar\boldsymbol{\nabla} + \frac{\hbar}{4m_0c^2}[\boldsymbol{\sigma} \times \boldsymbol{\nabla}V],$$

which includes the spin-orbit interaction term in a nonperturbative manner. Here, $\boldsymbol{\sigma}$ is the vector of the Pauli matrices that operate on spinors, and $V(\mathbf{r})$ is the crystal potential. The *ab initio* third-order **k** · **p** expansion at a TRIM in a centrosymmetric system [9,12] reads

$$H_{\mathbf{kp}} = H^{(0)} + H^{(1)} + H^{(2)} + H^{(3)},$$

where the zeroth-order term is just the band energy,

$$H^{(0)}_{n\nu m\mu} = \epsilon_n \delta_{mn}\delta_{\nu\mu},$$

and the linear term is

$$H^{(1)}_{n\nu m\mu} = \frac{\hbar}{m_0}\mathbf{k}\cdot\boldsymbol{\pi}_{n\nu m\mu}$$

with the matrix elements $\boldsymbol{\pi}_{n\nu m\mu} = \langle\Psi_{n\nu}|\boldsymbol{\pi}|\Psi_{m\mu}\rangle$. For two Kramers pairs of different parity, nth and mth, we turn the

phases such that $i\pi^{x(z)}_{n\uparrow m\downarrow}$ and/or $i\pi^{x(z)}_{n\uparrow m\uparrow}$ be real. The second- and third-order terms are

$$H^{(2)}_{n\nu m\mu} = \frac{\hbar^2 k^2}{2m_0}\delta_{mn}\delta_{\nu\mu} + \frac{\hbar^2}{m_0^2}\sum_{\alpha\beta}k_\alpha k_\beta D^{\alpha\beta}_{n\nu m\mu},$$

$$H^{(3)}_{n\nu m\mu} = \frac{\hbar^3}{m_0^3}\sum_{\alpha\beta\gamma}k_\alpha k_\beta k_\gamma T^{\alpha\beta\gamma}_{n\nu m\mu}$$

with $\alpha, \beta, \gamma = x, y, z$. Here, the coefficients are

$$D^{\alpha\beta}_{n\nu m\mu} = \frac{1}{2}\sum_{l\eta}\pi^\alpha_{n\nu l\eta}\pi^\beta_{l\eta m\mu}\left(\frac{1}{\Delta_{nl}} + \frac{1}{\Delta_{ml}}\right),$$

$$T^{\alpha\beta\gamma}_{n\nu m\mu} = -\frac{1}{2}\sum_{l\eta,m'\mu'}\left[\frac{\pi^\alpha_{n\nu l\eta}\pi^\beta_{l\eta m'\mu'}\pi^\gamma_{m'\mu'm\mu}}{\Delta_{ml}\Delta_{m'l}} + \frac{\pi^\alpha_{n\nu m'\mu'}\pi^\beta_{m'\mu'l\eta}\pi^\gamma_{l\eta m\mu}}{\Delta_{nl}\Delta_{m'l}}\right] + \frac{1}{2}\sum_{l\eta,l'\eta'}\pi^\alpha_{n\nu l\eta}\pi^\beta_{l\eta l'\eta'}\pi^\gamma_{l'\eta'm\mu}\left[\frac{1}{\Delta_{nl}\Delta_{nl'}} + \frac{1}{\Delta_{ml}\Delta_{ml'}}\right],$$

where $\Delta_{nl} = \epsilon_n - \epsilon_l$, and the indices $l\eta$ and $l'\eta'$ number the states in set B, i.e., run over all the states of the original Hilbert space ($\approx$5000 Kramers pairs) excluding those forming the $\mathbf{k}\cdot\mathbf{p}$ basis—the subspace A. Since the states in both set A and set B exhibit all the symmetry properties of the TRIM-projected *ab initio* Hamiltonian, it is the symmetry of the system that is ultimately responsible for the nonzero matrix elements of the effective Hamiltonian in the final symbolic form.

APPENDIX B: PARAMETERS OF THE 2 × 2 HAMILTONIAN

The analytical transformation of the four-band Hamiltonian (2) by means of the Löwdin partitioning leads to the following expressions for the parameters of the two-band Hamiltonian (7):

$$\alpha^{(3)} = \alpha_1^{(3)} - \frac{2M_0\zeta^{(1)}}{\Delta_{21}} - \frac{\zeta^{(1)2}}{\Delta_{21}^2}\left[\alpha_1^{(1)} - \alpha_2^{(1)}\right],$$

$$\alpha^{(5)} = -\frac{2}{\Delta_{21}}[M_0\zeta^{(3)} - \eta D] - \frac{1}{\Delta_{21}^2}\left(\left[M_0^2 + 2\zeta^{(1)}\zeta^{(3)}\right]\left[\alpha_1^{(1)} - \alpha_2^{(1)}\right] + \alpha_1^{(1)}D^2 + 2M_0\zeta^{(1)}[M_1 - M_2] + \zeta^{(1)2}\left[\alpha_1^{(3)} - \alpha_2^{(3)}\right]\right),$$

$$\alpha^{(7)} = \frac{1}{\Delta_{21}^2}\{2[M_1 - M_2][\eta D - M_0\zeta^{(3)}] - 2W_2[M_0 D + \zeta^{(1)}(\theta - \eta)]\}$$
$$+ \frac{1}{\Delta_{21}^2}\{\left[\alpha_1^{(3)} - \alpha_2^{(3)}\right]\left[M_0^2 + 2\zeta^{(1)}\zeta^{(3)}\right] - \left[\alpha_1^{(1)} - \alpha_2^{(1)}\right]\zeta^{(3)2} - \alpha_1^{(3)}D^2 - \alpha_1^{(1)}(\theta^2 + \eta^2) + 2\alpha_2^{(1)}\theta\eta\},$$

$$W^{(0)} = W_1 - \zeta^{(1)}D/\Delta_{21},$$

$$W^{(2)} = \frac{1}{\Delta_{21}}[M_0(\theta - \eta) - \zeta^{(3)}D] - \frac{1}{\Delta_{21}^2}\left(\zeta^{(1)2}[W_1 + W_2] + \zeta^{(1)}D[M_1 - M_2] + \alpha_2^{(1)}\zeta^{(1)}[\theta - \eta] - \alpha_2^{(1)}M_0 D\right),$$

$$W^{(4)} = \frac{1}{\Delta_{21}^2}\{(\theta - \eta)\left[M_0(M_1 - M_2) - \alpha_2^{(1)}\zeta^{(3)} - \alpha_2^{(3)}\zeta^{(1)}\right] - \zeta^{(3)}D[M_1 - M_2]\}$$
$$- \frac{1}{\Delta_{21}^2}\left(M_0^2[W_1 - W_2] + [W_1 + W_2][D^2 + 2\zeta^{(1)}\zeta^{(3)}] - \alpha^{(3)}M_0 D\right),$$

$$M^{(0)} = M_1 - \zeta^{(1)2}/\Delta_{21},$$

$$M^{(2)} = -\frac{1}{\Delta_{21}}\left(M_0^2 + D^2 + 2\zeta^{(1)}\zeta^{(3)}\right) - \frac{1}{\Delta_{21}^2}\left(\zeta^{(1)2}[M_1 - M_2] + 2\zeta^{(1)}M_0\left[\alpha_1^{(1)} - \alpha_2^{(1)}\right]\right),$$

$$M^{(4)} = -\frac{1}{\Delta_{21}}(\theta^2 + \eta^2 + \zeta^{(3)2}) - \frac{1}{\Delta_{21}^2}\left([M_1 - M_2]\left[M_0^2 + D^2 + 2\zeta^{(1)}\zeta^{(3)}\right]\right)$$
$$- \frac{2}{\Delta_{21}^2}\{\zeta^{(3)}M_0\left[\alpha_1^{(1)} - \alpha_2^{(1)}\right] - D\left(\alpha_1^{(1)}\eta - \alpha_2^{(1)}\theta\right) + \zeta^{(1)}M_0\left[\alpha_1^{(3)} - \alpha_2^{(3)}\right] + \zeta^{(1)}D[W_1 + W_2]\},$$

$$\gamma^{(5)} = -\frac{2\theta D}{\Delta_{21}} - \frac{D^2 \alpha_2^{(1)}}{\Delta_{21}^2},$$

$$\gamma^{(7)} = -\frac{1}{\Delta_{21}^2} \big(2\theta D[M_1 - M_2] + 2W_2[M_0 D + \theta\zeta^{(1)}] - \alpha_1^{(1)}\theta\eta + \alpha_2^{(1)}\theta^2 + \alpha_2^{(3)}D^2 \big),$$

$$\mathcal{N} = -\frac{\theta\eta}{\Delta_{21}} + \frac{D}{\Delta_{21}^2} \big(\zeta^{(1)}[W_1 + W_2] + \alpha_1^{(1)}\theta - \alpha_2^{(1)}\eta \big),$$

$$\xi = \frac{1}{\Delta_{21}^2} \big(\eta^2 \alpha_2^{(1)} - 2\eta\zeta^{(1)}W_2 - \alpha_1^{(1)}\eta\theta \big), \ \Delta_{21} = \epsilon_2 - \epsilon_1.$$

[1] H. Zhang, C.-X. Liu, X.-L. Qi, X. Dai, Z. Fang, and S.-C. Zhang, Topological insulators in Bi_2Se_3, Bi_2Te_3 and Sb_2Te_3 with a single Dirac cone on the surface, Nat. Phys. **5**, 438 (2009).

[2] C.-X. Liu, X.-L. Qi, H. J. Zhang, X. Dai, Z. Fang, and S.-C. Zhang, Model Hamiltonian for topological insulators, Phys. Rev. B **82**, 045122 (2010).

[3] S. LaShell, B. A. McDougall, and E. Jensen, Spin Splitting of an Au(111) Surface State Band Observed with Angle Resolved Photoelectron Spectroscopy, Phys. Rev. Lett. **77**, 3419 (1996).

[4] Y. H. Wang, D. Hsieh, D. Pilon, L. Fu, D. R. Gardner, Y. S. Lee, and N. Gedik, Observation of a Warped Helical Spin Texture in Bi_2Se_3 from Circular Dichroism Angle-Resolved Photoemission Spectroscopy, Phys. Rev. Lett. **107**, 207602 (2011).

[5] S. Basak, H. Lin, L. A. Wray, S.-Y. Xu, L. Fu, M. Z. Hasan, and A. Bansil, Spin texture on the warped Dirac-cone surface states in topological insulators, Phys. Rev. B **84**, 121401(R) (2011).

[6] P. Höpfner, J. Schäfer, A. Fleszar, J. H. Dil, B. Slomski, F. Meier, C. Loho, C. Blumenstein, L. Patthey, W. Hanke, and R. Claessen, Three-Dimensional Spin Rotations at the Fermi Surface of a Strongly Spin-Orbit Coupled Surface System, Phys. Rev. Lett. **108**, 186801 (2012).

[7] I. A. Nechaev and E. E. Krasovskii, Relativistic k · p Hamiltonians for centrosymmetric topological insulators from *ab initio* wave functions, Phys. Rev. B **94**, 201410(R) (2016).

[8] I. A. Nechaev and E. E. Krasovskii, Relativistic splitting of surface states at Si-terminated surfaces of the layered intermetallic compounds RT_2Si_2 (R=rare earth; T=Ir, Rh), Phys. Rev. B **98**, 245415 (2018).

[9] I. A. Nechaev and E. E. Krasovskii, Spin polarization by first-principles relativistic k · p theory: Application to the surface alloys $PbAg_2$ and $BiAg_2$, Phys. Rev. B **100**, 115432 (2019).

[10] I. A. Nechaev, S. V. Eremeev, E. E. Krasovskii, P. M. Echenique, and E. V. Chulkov, Quantum spin Hall insulators in centrosymmetric thin films composed from topologically trivial BiTeI trilayers, Sci. Rep. **7**, 43666 (2017).

[11] S. Schulz, I. A. Nechaev, M. Güttler, G. Poelchen, A. Generalov, S. Danzenbächer, A. Chikina, S. Seiro, K. Kliemt, A. Y. Vyazovskaya, T. K. Kim, P. Dudin, E. V. Chulkov, C. Laubschat, E. E. Krasovskii, C. Geibel, C. Krellner, K. Kummer, and D. V. Vyalikh, Emerging 2D-ferromagnetism and strong spin-orbit coupling at the surface of valence-fluctuating $EuIr_2Si_2$, npj Quantum Mater. **4**, 26 (2019).

[12] D. Y. Usachov, I. A. Nechaev, G. Poelchen, M. Güttler, E. E. Krasovskii, S. Schulz, A. Generalov, K. Kliemt, A. Kraiker, C. Krellner, K. Kummer, S. Danzenbächer, C. Laubschat, A. P. Weber, J. Sánchez-Barriga, E. V. Chulkov, A. F. Santander-Syro, T. Imai, K. Miyamoto, T. Okuda, and D. V. Vyalikh, Cubic Rashba Effect in the Surface Spin Structure of Rare-Earth Ternary Materials, Phys. Rev. Lett. **124**, 237202 (2020).

[13] D. Niesner, T. Fauster, S. V. Eremeev, T. V. Menshchikova, Y. M. Koroteev, A. P. Protogenov, E. V. Chulkov, O. E. Tereshchenko, K. A. Kokh, O. Alekperov, A. Nadjafov, and N. Mamedov, Unoccupied topological states on bismuth chalcogenides, Phys. Rev. B **86**, 205403 (2012).

[14] J. A. Sobota, S.-L. Yang, A. F. Kemper, J. J. Lee, F. T. Schmitt, W. Li, R. G. Moore, J. G. Analytis, I. R. Fisher, P. S. Kirchmann, T. P. Devereaux, and Z.-X. Shen, Direct Optical Coupling to an Unoccupied Dirac Surface State in the Topological Insulator Bi_2Se_3, Phys. Rev. Lett. **111**, 136802 (2013).

[15] D. Niesner, S. Otto, T. Fauster, E. V. Chulkov, S. V. Eremeev, O. E. Tereshchenko, and K. A. Kokh, Electron dynamics of unoccupied states in topological insulators, J. Electron Spectrosc. Relat. Phenom. **195**, 258 (2014).

[16] C. Datzer, A. Zumbülte, J. Braun, T. Förster, A. B. Schmidt, J. Mi, B. Iversen, P. Hofmann, J. Minár, H. Ebert, P. Krüger, M. Rohlfing, and M. Donath, Unraveling the spin structure of unoccupied states in Bi_2Se_3, Phys. Rev. B **95**, 115401 (2017).

[17] I. Aguilera, C. Friedrich, and S. Blügel, Many-body corrected tight-binding Hamiltonians for an accurate quasiparticle description of topological insulators of the Bi_2Se_3 family, Phys. Rev. B **100**, 155147 (2019).

[18] E. E. Krasovskii, Accuracy and convergence properties of the extended linear augmented-plane-wave method, Phys. Rev. B **56**, 12866 (1997).

[19] E. E. Krasovskii, F. Starrost, and W. Schattke, Augmented fourier components method for constructing the crystal potential in self-consistent band-structure calculations, Phys. Rev. B **59**, 10504 (1999).

[20] D. D. Koelling and B. N. Harmon, A technique for relativistic spin-polarised calculations, J. Phys. C **10**, 3107 (1977).

[21] R. W. G. Wyckoff, *Crystal Structures* (Wiley, New York, 1964), Vol. 2.

[22] I. A. Nechaev, R. C. Hatch, M. Bianchi, D. Guan, C. Friedrich, I. Aguilera, J. L. Mi, B. B. Iversen, S. Blügel, P. Hofmann, and E. V. Chulkov, Evidence for a direct band gap in the topological

insulator Bi_2Se_3 from theory and experiment, Phys. Rev. B **87**, 121111(R) (2013).

[23] P.-O. Löwdin, A note on the quantum-mechanical perturbation theory, J. Chem. Phys. **19**, 1396 (1951).

[24] J. R. Schrieffer and P. A. Wolff, Relation between the Anderson and Kondo Hamiltonians, Phys. Rev. **149**, 491 (1966).

[25] R. Winkler, *Spin-Orbit Coupling Effects in Two-Dimensional Electron and Hole Systems* (Springer-Verlag, Berlin, 2003).

[26] L. Fu, Hexagonal Warping Effects in the Surface States of the Topological Insulator Bi_2Te_3, Phys. Rev. Lett. **103**, 266801 (2009).

[27] A multiple winding of the in-plane spin was recently observed at the Si-terminated surface of $TbRh_2Si_2$ (the